Mechanical Properties and Deformation Behavior in Hot-rolled 0.2C-1.5/3Al-8.5Mn-Fe TRIP steel: The Discontinuous TRIP Effect

Z.C. Li[a,b], R.D.K. Misra[b,*], Z.H. Cai[a], H.X. Li[a], H. Ding[a,*]

[a] School of Materials Science and Engineering,
Northeastern University, Shenyang, 110819, China

[b] Laboratory for Excellence in Advanced Steel Research,
Department of Metallurgical, Materials and Biomedical Engineering,
University of Texas at El Paso, El Paso, TX 79968, USA

Abstract

Mechanical properties and deformation behavior have been studied in two hot-rolled 0.2C-1.5Al-8.5Mn-Fe (1.5Al steel) and 0.2C-3Al-8.5Mn-Fe (3Al steel) transformation induced plasticity (TRIP) steels, subjected to an optimized quenching and tempering (Q&T) treatment. The study indicated that 1.5Al steel was characterized by excellent combination of ultimate tensile strength (UTS) of 1373 MPa, tensile elongation (TE) of 31.8%, and UTS×TE of 43.6 GPa%, where the superior mechanical properties are mainly attributed to the discontinuous TRIP effect. In contrast, 3Al steel indicated lower UTS, but higher TE of 34.5%, which resulted from the discontinuous TRIP effect and the cooperative deformation of δ-ferrite. The discontinuous TRIP effect is a consequence of varying degree of stability of austenite, which results from different austenite grain size, non-uniform C-content and Mn-distribution in lath-like austenite and blocky austenite.

Keywords: TRIP; mechanical properties; deformation behavior; carbon and manganese distribution

---

* Corresponding authors: E-mail: dinghuaneu@163.com (H. Ding); dmisra2@utep.edu (R.D.K. Misra).

© 2016. This manuscript version is made available under the Elsevier user license
http://www.elsevier.com/open-access/userlicense/1.0/

1. Introduction

Transformation induced plasticity (TRIP) steels with high strength, superior ductility, and good crashworthiness are potential candidates for automotive applications [1-2]. The increasing demand for energy conservation, environmental protection, and reduced weight of automobiles has led to significant interest in the development of new advanced high strength steels. Medium Mn-content (5-12%) transformation-induced plasticity (TRIP) steels are potential candidates for automotive applications, where the TRIP effect can be completely utilized [3-5].

A number of studies have been carried out on medium-Mn TRIP steel [6-9], which suggested that superior mechanical properties can be obtained with increase in Mn and C-content, because they increase the volume fraction of retained austenite. For example, Luo et al. [10] reported that Fe-5Mn-0.2C (wt.%) steel exhibited tensile strength of 850-950 MPa and ductility of 20-30%. Miller [11] reported that Fe-5.7Mn-0.1C (wt.%) steel was characterized by tensile strength of 878 MPa and total elongation of 34%. On the other hand, Merwin [12] achieved high tensile strength (1018 MPa) and large total elongation (32%) in Fe-7Mn-0.1C (wt.%) steel.

In recent studies, Al was added to medium-Mn TRIP steels to optimize austenite stability by suppressing the formation of cementite. Furthermore, Al in TRIP steels facilitated the presence of α-ferrite and δ-ferrite and contributed to excellent mechanical properties [13, 14]. In this regard, Suh et al. reported excellent combination of high tensile strength (1000 MPa) and ductility (30%) in Fe-6Mn-0.1C-3Al (wt.%) steel [15]. Cai et al. obtained tensile strength of 980 MPa and a total elongation of 33% in Fe-8Mn-0.2C-4Al (wt.%) steel [16]. Similarly, Park et al. [17] obtained tensile strength of 949 MPa and a total elongation of 54% in Fe-8Mn-0.2C-5Al (wt.%) steel. In another instance, Han et al. [18] obtained tensile strength of 1090 MPa and a total elongation of

40% in Fe-10Mn-0.14C-1.5Al steel.

Given that the effects of Al on austenite stability, work hardening behavior of medium-Mn TRIP steels continues to be unclear, the objective of the study described here is aimed at developing a scientific basis for obtaining excellent tensile strength and ductility in hot-rolled 0.2C-1.5/3Al-8.5Mn-Fe steels. Also, described is the microstructural evolution and mechanical properties to demonstrate the potential of proposed alloy design-processing relationship in obtaining desired mechanical properties. The stress-strain plot is characterized by serrations, which are of interest in medium-Mn TRIP steels. In the present work, we ascribe this phenomenon to the unique discontinuous TRIP effect involving stress relaxation and transfer during deformation with consequent enhancement in ductility.

2. Experimental

The nominal chemical composition of the two experimental steels was 0.2C-1.5Al-8.5Mn-Fe (wt.%) (1.5Al steel) and 0.2C-3Al-8.5Mn-Fe (wt.%) (3Al steel), and is listed in Table 1. The 40 kg experimental steel ingots were cast in a vacuum induction furnace. The ingots were heated at 1200℃ for 2 h, hot forged into rods of section size 100 mm×30 mm, then air cooled to room temperature (RT). Subsequently, the rods were soaked at 1200℃ for 2 h, hot-rolled to 4 mm thick strip in the temperature range of 1150-850℃, and finally air cooled to room temperature (RT).

A model proposed by De Moor et al. [19] was used to predict the amount of austenite stabilized at room temperature via enrichment with Mn, Al and C. It was further deduced that there exist a temperature in the intercritical region resulting in the maximum austenite retention at room temperature. The model provided guidance in optimizing the alloy composition. In this

regard, intercritical temperature range and phase transformations were studied by dilatometry. Dilatometry samples were solid cylindrical specimen of diameter 3 mm and length of 10 mm.

We recently [20-22] demonstrated that austenite reverted transformation (ART) annealing heat treatment (sample is accelerated cooled in water after austenization, then intercriticaly annealed for a long time and finally air cooled to room temperature) used for medium-Mn steels was not applicable to the experimental steel studied here. A long time annealing renders austenite too stable and weakens the TRIP effect. Thus, quenching and tempering (Q&T) was envisioned by us as an alternative and effective heat treatment [23-25]. The as-hot-rolled sheets were subjected to Q&T heat treatment. First, they were annealed in the intercritical temperature range for 1 h, followed by immediate quenching in water to room temperature. Second, the quenched samples were tempered at 200℃ for 20 min and then air cooled to ambient temperature. Tempering helps in relieving the internal stresses. It was demonstrated in our previous study [25] that carbon diffused from ferrite to austenite during tempering, which enhanced the stability of austenite, leading to superior ductility.

Tensile specimens of dimensions 12.5 mm width and gage length of 50 mm were machined from the heat-treated sheets with tensile axis parallel to the prior rolling direction. Tensile tests were carried out at room temperature using a universal testing machine (SANSCMT5000) at a constant crosshead speed of 3 $mm \cdot min^{-1}$. The samples were etched with 25% sodium bisulfite solution. Microstructural examination was carried out using scanning electron microscope (SEM) and electron probe micro-analyzer (EPMA). Microhardness measurements were carried out using Vicker hardness tester at a load of 50 kgf and the holding time of 10 s. The volume fraction of austenite was determined by X-ray diffraction (XRD) using CuK_{α} radiation [26] and

involved the use of integrated intensities of $(200)_\alpha$ and $(211)_\alpha$ peaks and those of $(200)_\gamma$, $(220)_\gamma$ and $(311)_\gamma$ peaks. The volume fraction of austenite V_A was calculated using equation [27]:

$$V_A = 1.4I_\gamma / (I_\alpha + 1.4I_\gamma) \quad (1)$$

where I_γ is the integrated intensity of austenite and I_α is the integrated intensity of α-phase.

3. Results

3.1 Composition design and intercritical temperature

The phase fraction of 1.5Al steel and 3Al steel based on an equilibrium thermodynamic analysis [19] predicted by Thermo-Calc are presented in Figs. 1a and 1b, respectively, and the predicted equilibrium austenite fractions were used as input to the model. Prediction of austenite composition was also made using Thermo-Calc, and the predicted C, Al and Mn-content in austenite of 1.5Al steel and 3Al steel are presented in Figs. 1c and 1d, respectively. The resulting predicted fraction of stabilized austenite of 1.5Al steel and 3Al steel as a function of annealing temperature are shown in Figs. 1e and 1f, respectively. A pronounced peak is observed at ~660℃, resulting in maximum austenite fraction (~78%) retained at room temperature for 1.5Al steel. For 3Al steel, a pronounced peak is observed at ~730℃, resulting in maximum austenite fraction (~53%) retained at room temperature.

The phase transformation temperatures were determined by dilatometer experiments. The dilatometric plots of the two experimental steels are presented in Fig. 2. After thermal expansion during the heating stage (30–1100℃) at the rate of 20℃/s, the sample was held at 1100℃ for 3 min. It is clear that no transformation took place in the two samples during fast cooling, at the rate of 100℃/s, until martensite start (Ms) temperature. The intercritical temperature range of 1.5 Al steel and 3 Al steel were 586-749℃ and 618-863℃, respectively, as marked in Fig. 2.

The dilatometer was used to study 1.5Al steel quenched from different temperatures, as shown in Fig. 3a. It is clear that Ms temperature increases with increase in quenching temperature (Fig. 3b). Ms temperature was below the room temperature when the quenching temperature was below 670℃. As indicated by XRD data (Fig. 4), for 1.5Al steel, the austenite fraction decreased significantly when quenched from 700-750℃. Thus, the Q&T treatment is also on the basis of results of thermal dilation experiment.

3.2 Microstructure

The SEM micrographs of hot-rolled 1.5Al steel heat-treated at different temperatures are presented in Fig. 5. Figs. 5a and 5b describe the microstructure of samples quenched from 600℃ and 650℃, respectively, followed by tempering at 200℃. The microstructural constituents consisted of acicular α-ferrite (α-F) and austenite (A) as the dominant phase. It is clear that austenite grain size of the two samples increased with increase in quenching temperature. The austenite of the sample quenched from 600℃ mainly consisted of lath-like austenite, while blocky austenite was present in the sample quenched from 650℃. With increase in annealing temperature, the volume fraction of austenite was increased and austenite grain size increased. As a result, some austenite islands merged and grain growth occurred during annealing in the intercritical region with increase in annealing temperature, which led to the presence of blocky austenite. When the sample was quenched from 700℃ and 750℃, respectively, as marked in Figs. 5c and 5d, austenite was significantly decreased because of extensive martensitic (M) transformation.

Fig. 6 shows SEM micrographs of heat-treated 3Al steel. Because of higher Al content, δ-ferrite was obtained. As shown in Figs. 6a-c, the microstructural constituents of the samples

quenched from 650℃, 700℃ and 750℃ respectively, followed by tempering at 200℃ consisted of α-ferrite (α-F), δ ferrite (δ-F) and austenite (A). The volume fraction of blocky austenite was increased with increased quenching temperature. For the sample quenched from 800℃, the microstructural constituents were α-F, δ-F, austenite and martensite (M) (Fig. 6d). The two kinds of ferrite differed in morphology, but also in microhardness (Table 2).

The variation in the volume fraction of austenite obtained from XRD is summarized in Fig. 4. 1.5Al steel had a high austenite fraction of 63-80 vol.% in the temperature range of 600-650℃, followed by drastic decrease to 34-20 vol.%, when quenching was carried out in the temperature range of 700-750℃ because of martensitic transformation (as shown in Figs. 5c and 5d). Similar trend in the austenite fraction was observed in 3Al steel. It is obvious that 3Al steel had lower austenite content than 1.5Al steel.

3.3 Mechanical properties

The mechanical properties of 1.5Al steel and 3 Al steel are summarized in Fig. 7. The variation in yield strength (YS), ultimate tensile strength (UTS) and total elongation (TE) of the two steels were similar. The ultimate tensile strength (UTS) increased continuously with increase in temperature, but the total elongation (TE) of 1.5Al steel and 3Al steel increased with increase in temperature after attaining peak value of 31.8% at 650℃（1.5Al-650 sample) and 34.5% at 750℃（3Al-750 sample), respectively. The yield strength (YS) of 1.5Al steel and 3Al steel increased with increase in temperature after attaining minimum value of 645 MPa on quenching from 650℃（1.5Al-650 sample) and 652 MPa on quenching from 750℃（3Al-750 sample), respectively, (Fig. 7a). For 1.5Al steel, the grain size of austenite increased with increase in temperature on quenching from temperatures below 650℃. The yield strength (YS) and austenite

grain size followed Hall-Petch relationship. However, the YS increased after quenching from 700℃ was because of the high fraction of martensite. Thus, 1.5Al steel sample quenched from 650℃ exhibited lowest yield strength. The variation in YS of 3Al samples can be interpreted in a similar way.

Compared to the 3Al steel, 1.5Al steel had a significantly higher UTS of 1160-1500 MPa than 3Al steel (900-1200 MPa). The 1.5Al steel sample quenched from 650℃ exhibited superior mechanical properties among all the samples, and was characterized by excellent combination of TE of 31.8%, UTS of 1373 MPa, and UTS×TE of 43.6 GPa%, which are significantly superior to the values reported for the medium Mn-content TRIP steels, as shown in Table 3 [12,15,16,22,28-30]. The two steels were characterized by significantly superior mechanical properties compared to the data reported for other medium-Mn TRIP steels by adopting Q&T treatment. Moreover, Q&T treatment is simple and easy to adopt. Thus, it is a convenient and effective heat treatment.

It is clear that, 1.5Al steel had a significantly higher UTS than 3Al steel, while 3Al steel exhibited higher ductility. Desired mechanical properties can be obtained by optimizing the Al-content. The reason underlying the superior mechanical properties of 1.5Al steel sample quenched from 650℃ and the difference in the mechanical properties between the two steels can be further elucidated by studying the stability of austenite and their deformation mechanisms.

4. Discussion

4.1 The critical factors governing UTS

The variation in UTS was explained using the rule of mixtures proposed by Embury and Bouaziz [31].

$$\sigma = f_\alpha \sigma_\alpha + f_\gamma \sigma_\gamma + f_m \sigma_m \quad (2)$$

where σ_α, σ_γ, σ_m are the flow stresses and f_α, f_γ, f_m, are volume fraction of ferrite, austenite and martensite, respectively. However, the rule is not applicable in the case of 1.5Al and 3Al steels. For the two steels, there were significant differences in the constituents of the microstructure between the samples quenched from different temperatures.

In the case of 1.5Al steel, the samples quenched from 550-650℃ consisted of austenite and ferrite. As regards, the samples quenched from 700-750℃, the microstructural constituents consisted of ferrite, martensite and austenite. The microstructure of samples quenched from 550-650℃ and from 700-750℃ were different. Moreover, it was found that the newly generated martensite, namely, transformed martensite, evolved during tensile deformation had a higher microhardness than the original martensite formed during quenching. The original martensite and the newly generated martensite are both expected contribute to UTS.

Thus, we propose the use of a modified rule of mixtures:

$$\sigma_F = f_\alpha \sigma_\alpha + (f_\gamma - f_{nm}) \sigma_\gamma + f_{nm} \sigma_{nm} + f_m \sigma_m \quad (3)$$

where σ_{nm} is the flow stress and f_{nm} is volume fraction of newly generated martensite during tensile deformation. Based on SEM micrographs (Fig. 5) and XRD results (Fig. 4), 1.5Al steel samples quenched from 550-650℃ consisted of austenite and ferrite and the transformation ratio of austenite increased with increase in quenching temperature. Thus, σ_F is determined by the austenite fraction and TRIP effect. The corresponding UTS increased from 1163 MPa to 1373 MPa. Meanwhile, due to the TRIP effect, the TE increased with temperature. The samples quenched from 700-750℃ consisted of original martensite which had a high microhardness. The σ_F depends on the fraction of martensite. Because of the increased martensite fraction, the

corresponding UTS increased from 1373 MPa to 1502 MPa and the TE decreased with temperature. The variation in UTS and TE of 3Al samples can be interpreted in a similar way. Thus, the ultimate tensile strength (UTS) increased continuously with increase in intercritical temperature because of the enhanced TRIP effect induced during tensile deformation (consistent with Fig. 4) and increased martensite fraction.

Combining XRD results (Fig. 4) and mechanical properties (Fig. 7), two interesting phenomena were observed. First, 1.5Al-600 sample comprised of 63 vol.% austenite. In contrast, 3Al-750 sample comprised of 58 vol.% austenite. Interestingly, the corresponding TE for 3Al-750 sample was significantly higher than 1.5Al-600 sample (1.5Al-600: 23.2%, 3Al-750: 34.5%). It is worth noting that the austenite fraction in 1.5Al-650 sample is ~80 vol.%, while 3Al-750 sample has a lower austenite fraction of 58 vol.%. Furthermore, the transformation ratio of austenite in 1.5Al-650 sample (68.3%) was higher than 3Al-750 sample (65.7%) during the tensile test. But the corresponding TE for 3Al-750 sample was higher than 1.5Al-650 sample (1.5Al-650: 31.8%, 3Al-750: 34.5%). The underlying reason for the two phenomena can be elucidated by studying the work-hardening behavior, austenite stability and deformation behavior.

4.2 Deformation behavior and austenite stability

As shown in Figs. 8a and 8b, the work-hardening behavior of 1.5Al steel and 3Al steel exhibited three stages of work hardening rate (WH) evolution: in stage 1, WH rapidly decreases; then decreases gently (stage 2) before finally decreases quickly again (stage 3) with increasing tensile strain. The majority of studies reported in the literature [32-34] primarily relate the first stage to deformation of ferrite, the final stage is probably associated with deformation of ferrite

and martensite as the martensitic transformation is inactive in this stage. The stage 2 characterized by a gradual decrease, unlike the sharp decline in stages 1 and 3, is a consequence of TRIP effect [34] accompanied by the deformation of ferrite. Thus, the second intermediate stage was attributed to the occurrence of TRIP effect. It is inferred that the work hardening ability in stage 2 is related to the stability of austenite. In the attempt to quantify this behavior, equation (4) was used [35-36]:

$$f_\gamma = f_{\gamma 0} \exp(-k\varepsilon) \quad (4)$$

In equation (4), $f_{\gamma 0}$, f_γ and k are the initial austenite fraction, the austenite fraction at strain ε, and the mechanical stability of austenite, respectively. A higher value of k corresponds to lower austenite stability. Fig. 9 is the plots of parameter k with quenching temperatures. It is clear that the value of k increases with increase in temperature, implying lower austenite stability. From the numerical results of the 1.5Al steel samples, 1.5Al-650 sample with the largest k value (k=4.3) exhibited the lowest austenite stability. In 3Al steel samples, 3Al-750 sample had the largest k-value (k=3.9). In the 1.5Al steel, the sample with higher k-value, the WH decreases more gently and corresponds to a larger strain region in stage 2, which indicates relatively strong work hardening ability. 3Al steel samples had similar variation. 3Al-750 sample had higher k-value (k=3.9) than 1.5Al-600 sample (k=3.1), corresponding to the larger value of WH and consequently higher ductility.

The true stress-strain plots are presented in Fig. 10. Interestingly, an obvious difference is that the observed serrations in the plots of 1.5Al-650 sample and 3Al-750 sample, corresponds to the observed serrations in the work hardening rate plots in stage 2 presented in Fig. 8. SEM micrograph of 1.5Al-650 sample after tensile fracture is presented in Fig. 11. It is clear that

ferrite (F) was squeezed to fill the intermediate space and appears to spill over. Thus, significant deformation occurred in ferrite because of volume expansion associated with martensitic transformation. Work hardening rate, true stress-strain plot and comparison between work hardening rate and true stress-strain plots of 1.5Al-650 sample are presented in Fig. 12. As shown in Fig. 12c, the serrations of stress–strain plot are characterized by abrupt stress drops to below the general level of the flow curve (point a_1 drops to a_2), followed by a rise in the stress (point a_2 rises to a_3). Then the stress rises with fluctuations (point a_3 rises to b_1). Studying stage 2 of work hardening rate in Fig. 12c enables us to develop a good understanding of the interesting observed serration phenomenon. In the first stage (a_1–a_3), martensitic transformation is activated when a certain critical stress is attained, and then transformation continuously takes place in the remaining austenite of similar stability. In this stage, the work hardening rate (WH) increases rapidly because of the TRIP effect and corresponds to an abrupt drop in stress followed by a gradual increase. This abrupt drop is attributed to the onset of the TRIP effect which relaxes and transfers the local stress to the surrounding ferrite and austenite. On the other hand, the gradual increase is a consequence of competition between the increase in tensile stress and stress relaxation and transfer induced by the TRIP effect. When the stress rebounds to the point a_3, the austenite in the deformation zone with similar degree of stability is transformed to martensite. The second stage (a_3–b_1) concerns accumulation of stress. In this stage, the work hardening rate (WH) decreases and rebounds when the stress is sufficiently large (point b_1), initiating a second round of TRIP effect, corresponding to the stage b_1-b_3. Considering that the stress at point b_1 is larger than at a_1, it is highly likely that austenite with a higher degree of stability is activated to transform. The TRIP effect that occurs discontinuously in the 1.5Al-650 sample during tensile. In

conclusion, the serrated behavior in true stress-strain plot is attributed to the discontinuous TRIP effect involving stress relaxation and transfer during deformation with consequent enhancement in ductility.

It is clear that the superior mechanical properties of 1.5Al-650 and 3Al-750 samples are attributed to discontinuous TRIP effect. Based on the XRD results, 1.5Al-650 sample (k=4.3) had higher austenite fraction, higher transformation ratio of austenite and more obvious TRIP effect than than 3Al-750 sample, 1.5Al-650 sample should have higher ductility contributed by discontinuous TRIP effect. However, as mentioned above, 3Al-750 sample had superior ductility than 1.5Al-650 sample. Thus, besides discontinuous TRIP effect, there are other factors contributed to ductility in 3Al-750 sample. Al in TRIP steels encourages the growth of intercritical ferrite [37] and facilitates the presence of δ-ferrite during solidification and contributes to excellent tensile properties [13,14]. δ-ferrite is a soft phase with good ductility [16,24,25] was present in 3Al steel, while it was absent in 1.5Al steel. As a consequence, the deformation of δ-ferrite also contributed to superior ductility in 3Al-750 sample.

Thus, it is deduced that the ductility in 3Al-750 sample is a cumulative contribution of discontinuous TRIP effect and the cooperative effect of δ-ferrite. For 1.5Al-650 sample, discontinuous TRIP effect played a leading role without the cooperative effect of δ-ferrite. Based on the discussion above, TRIP effect is primarily influenced by austenite stability rather than austenite fraction.

4.3 The critical factor governing austenite stability

SEM micrograph of 1.5Al-650 sample after tensile deformation in the vicinity of the fracture position is presented in Fig 11. It is obvious that the morphology of residual austenite is

mainly granular and small lath-like austenite. Comparing with the microstructure prior to the tensile test (Fig. 5b), it suggests that only the granular and lath-like austenite was retained but blocky austenite disappeared. Thus, it is inferred that the blocky austenite has lower stability than granular and lath-like austenite. It is known that the stability of austenite depends on factors including chemical composition, grain size [38-42], and morphology of austenite. The chemical composition has a strong influence on austenite stability [28, 43]. An increase in C-content and Mn-content, which are strong austenite stabilizers, increases the stability of austenite at room temperature.

Fig. 13 shows the micrograph of 1.5Al-650 sample and the corresponding carbon concentration and manganese partitioning in blocky austenite and lath-like austenite by EPMA. Micrograph of 1.5Al-650 sample and the corresponding distribution of carbon and manganese by EPMA are presented in Figs. 13a, 13b and 13c, respectively. We compared the region marked with a rectangle with the region marked with an oval circle in Figs. 13a, 13b and 13c. It is clear that carbon and manganese content in granular and lath-like austenite was higher than the blocky austenite. Figs. 13d, 13e and 13f show micrograph and the corresponding concentration of C and Mn in lath-like and blocky austenite grains, respectively. EPMA was used to estimate approximate partitioning of C and Mn. The statistical results of thirty randomly selected grains presented in Figs. 13d, 13e and 13f indicated that lath-like austenite had a higher C and Mn-content than blocky austenite. It is clear that higher C and Mn-content present in lath-like austenite, can explain higher austenite stability. Based on the above analysis, it is implied that the different austenite grain size, non-uniform C-content and Mn-distribution in lath-like austenite and blocky austenite resulted in different degree of stability of austenite, because of which

serrations were observed in true stress-strain plots, serrated work-hardening behavior was observed in stage 2 and led to discontinuous TRIP effect in 1.5Al-650 and 3Al-750 samples. The blocky austenite transformed more easily to martensite during the tensile test.

5. Conclusions

Microstructural evolution, mechanical properties, work hardening behavior and the stability of austenite in the 0.2C-1.5, 3Al-8.5Mn-Fe steels was studied in detail. The main conclusions are as follows:

(1) The hot- rolled 1.5Al-650 sample with a high volume fraction of austenite (~ 80 vol.%) exhibited best combination of mechanical properties, and was characterized by excellent combination of TE of 31.8%, UTS of 1373 MPa, and UTS×TE of 43.6 GPa%, which were significantly superior to a number of previously studied similar Mn-content TRIP steels.

(2) The highest ductility in 3Al-750 sample was influenced by discontinuous TRIP effect and cooperative deformation effect δ-ferrite. While discontinuous TRIP effect played a leading role without the cooperative effect of δ-ferrite in 1.5Al-650 sample, and contributed to tensile properties. Discontinuous TRIP effect, which primarily depends on the different degree of austenite stability, played a positive role in ductility.

(3) Based on the analysis of work hardening behavior, it was observed that austenite stability decreased with increase in temperature because of the increase in austenite grain size. Lath-like austenite had higher stability than blocky austenite. The varying degree of stability in the austenite phase resulted from the different austenite grain size, non-uniform C-content and Mn-distribution in lath-like austenite and blocky austenite.

Acknowledgements

The present study was financially supported by the National Natural Science Foundation of China (No: 51031001), National Science Foundation for Young Scientists of China (No: 51501035) and Chinese Postdoctoral Science Foundation (2015M580230). R.D.K.M. gratefully acknowledges support from University of Texas at El Paso, USA and by National Science Foundation, USA through Grant #DMR1458074.

References

[1] S. Lee, S.J. Lee, B.C. De Cooman, Scripta Mater. 65 (2011) 225-228.

[2] J. Shi, X.J. Sun, M.Q. Wang, W.J. Hui, H. Dong, W.Q. Cao, Scripta Mater. 63 (2010) 815-818.

[3] N. Nakada, K. Mizutani, T. Tsuchiyama, S. Takaki, Acta Mater. 65 (2014) 251-258.

[4] S. Lee, S-J Lee, S.S. Kumar, K. Lee, B.C. De Cooman, Metall. Mater. Trans. A. 42A (2011) 3638-3651.

[5] P.J. Gibbs, E. De Moor, M.J. Merwin, B. Clausen, J.G. Speer, D.K. Matlock, Metall. Mater. Trans. A. 42A (2011) 3691-3702.

[6] M.J. Santofimia, J.G. Speer, A.J. Clarke, L. Zhao, J. Sietsma, Acta Mater. 57 (2009) 4548-4557.

[7] G. Thomas, Metal. Trans. A. 9A (1978) 439-450.

[8] S.H. Li, W.J. Dan, W.G. Zhang, Z.Q. Lin, Comp. Mater. Sci 40 (2007)292-299.

[9] T. Bhattacharyya, S.B. Singh, S. Das, A. Haldar, D. Bhattacharjee, Mater. Sci. Eng. A. 528 (2011) 2394-2400.

[10] Y. Luo, J.M. Peng, H.B. Wang, X.C. Wu, Mater. Sci. Eng. A. 527 (2010) 3433-3437.

[11] R.L. Miller, Metall Trans. 3A(1972) 905-912.

[12] M.J. Merwin, Mater, Sci. Forum. 539-543(2007) 4327-4332.

[13] H.L. Yi, S.K. Ghosh, W.J. Liu, K.Y. Lee, H.K.D.H. Bhadeshia, Mater. Sci. Technol. 26 (2010) 817-823.

[14] S. Chatterjee, M. Murugananth, H.K.D.H. Bhadeshia, Mater. Sci. Technol. 23 (2007) 819-827.

[15] D.W. Suh, S.J. Park, T.H. Lee, C.S. Oh, S.J. Kim, Metall. Mater. Trans. A 41A (2010) 397-408.

[16] Z.H. Cai, H. Ding, Z.Y. Ying, R.D.K. Misra, J. Mater. Eng. Perform. 23 (2014) 1131-1137.

[17] S.J. Park, B. Hwang, K.H. Lee, T.H. Lee, D.W. Suh, H.N. Han, Scripta Mater. 68 (2013) 365-369.

[18] Q.H. Han, Y.L. Zhang, L. Wang, Metall. Mater. Trans. A. 46A (2015) 1917-1926.

[19] E. De Moor, D.K. Matlock, J.G. Speer, M.J. Merwin, Scripta Mater. 64(2011) 185-188.

[20] W.J. Dan, S.H. Li, W.G. Zhang, Z.Q. Lin, Mater. Design. 29 (2008) 604-612.

[21] W.Q. Cao, C. Wang, J. Shi, M.Q. Wang, W.J. Hui, H Dong, Mater. Sci. Eng. A 528 (2011) 6661-6666.

[22] G.B. Olson, M. Cohen, Metall Trans A, 6A (1975) 791-795.

[23] Z.H. Cai, H. Ding, X. Xue, Q.B. Xin, Mater. Sci. Eng. A 560 (2013) 388-395.

[24] Z.H. Cai, H. Ding, X. Xue, J. Jiang, Q.B. Xin, R.D.K. Misra, Scripta Mater. 68 (2013) 865-868.

[25] Z.H. Cai, H. Ding, R.D.K. Misra, H. Kong, H.Y. Wu, Mater. Sci. Eng. A. 595 (2014) 86-91.

[26] G.N. Haidemenopoulos, A.N. Vasilakos, J. Alloy. Compd 247 (1997) 128-133.

[27] B.K. Jha, Ram. Avtar, V. Sagar Dwivedi, Trans. Indian. Inst. Met. 49 (1996) 133-142.

[28] H.F. Xu, J. Zhao, W.Q. Cao, J. Shi, C.Y. Wang, J. Li, H. Dong, ISIJ. Int. 52 (2012) 868-873.

[29] S. Zhang, K.O. Findley, Acta Mater. 61 (2013) 1895-1903.

[30] M.I. Latypov, S. Shin, B.C. De Cooman, H.S. Kim, Acta Mater. 108 (2016) 219-228.

[31] D. Embury, O. Bouaziz, Annu. Rev. Mater. Res. 40 (2010) 213-241.
[32] B.K. Jha, V. Ram Avtar, Sagar Dwivedi, V. Ramaswamy, J. Mater. Sci. Lett. 6 (1987) 891-893.
[33] W.J. Dan, S.H. Li, W.G. Zhang, Z.Q. Lin, Mater. Des. 29 (2008) 604-612.
[34] A. Arlazarov, M. Gouné, O. Bouaziz, A. Hazotte, G. Petitgand, P. Barges, Mater. Sci. Eng. A 542 (2012) 31-39.
[35] K. Sugimoto, M. Kobayashi, S. Hashimoto, Metall. Mater. Trans. A 23A (1992) 3085-3091.
[36] Z.H. Cai, H. Ding, H. Kamoutsi, G.N. Haidemenopoulos, R.D.K. Misra, Mater. Sci. Eng. A 654 (2016) 359-367.
[37] D.W. Suh, S.J. Park, C.S. Oh, S.J. Kim, Scripta Mater. 57 (2007) 1097-1100.
[38] R.D.K. Misra, V.S.A. Challa, P.K.C. Venkatsurya, Y.F. Shen, M.C. Somani, L.P. Karjalainen, Acta Mater. 84 (2015) 339-348.
[39] R.D.K. Misra, X.L. Wan, V.S.A. Challa, M.C. Somani, L.E. Murr, Mater. Sci. Eng. A 626 (2015) 41-50.
[40] F.Z. Bu, X.M. Wang, S.W. Yang, C.J. Shang, R.D.K. Misra, Mater. Sci. Eng. A 620 (2014) 22-29.
[41] V.S.A. Challa, X.L. Wan, M.C. Somani, L.P. Karjalainen, R.D.K. Misra, Scripta Mater. 86 (2014) 60-63.
[42] R.D.K. Misra, P.K.C. Venkatsurya, M.C. Somani, L.P. Karjalainen, Metall. Mater. Trans. A 43A (2012) 5286-5297.
[43] S.J. Lee, S. Lee, B.C. De Cooman, Scripta Mater. 64 (2011) 649-652.

Figure captions

Fig. 1. Schematic illustration of the predictive model development for austenite stabilization as a function of temperature for 1.5Al steel and 3Al steel. (a)-(b) phase fractions, (c)-(d) C, Al and Mn-content in austenite and (e)-(f) calculated retained austenite fractions.

Fig. 2. Dilatometric plots for the experimental steels. (a) 1.5Al steel and (b) 3Al steel.

Fig. 3. Dilatometric plots and the evolution of *Ms* for 1.5Al steel on quenching from 650℃, 670℃, 700℃, 750℃, 800℃, 850℃and 900℃. (a) dilatometric plots and (b) evolution of *Ms*.

Fig. 4. Austenite fraction in undeformed and fractured samples of 1.5Al steel and 3Al steel heat-treated at different temperatures.

Fig. 5. SEM micrographs of hot-rolled 1.5Al samples after quenching from different temperatures. (a) 600℃, (b) 650℃, (c) 700℃ and (d) 750℃.

Fig. 6. SEM micrographs of hot-rolled 3Al samples after quenching from different temperatures. (a) 650℃, (b) 700℃, (c) 750℃ and (d) 800℃.

Fig. 7. Comparisons of tensile properties between 1.5Al steel and 3Al steel. (a) YS of the 1.5 Al steel and 3Al steel, (b) UTS and TE of 1.5Al steel, (c) UTS and TE of 3Al steel and (d) UTS × TE comparisons of the 1.5 Al steel and 3Al steel. (YS-yield strength, UTS-ultimate tensile strength, TE-total elongation).

Fig. 8. Work hardening rate of 1.5Al, 3Al steels quenched from different temperatures. (a) 1.5Al steel and (b) 3Al steel.

Fig. 9. The plots of parameter *k* for 1.5Al and 3Al steel samples intercritically hardened at different temperatures.

Fig. 10. True strain-stress plots of 1.5Al steel and 3Al steel quenched from different temperatures. (a) 1.5Al steel and (b) 3Al steel.

Fig. 11. SEM micrograph of 1.5Al-650 sample after tensile fracture.

Fig. 12. True stress-strain curve and work-hardening rate plot of 1.5Al-650 sample: (a) true stress-strain curve, (b) work-hardening rate and (c) partial magnification of the true stress-strain and work-hardening rate plots.

Fig. 13. Micrograph of 1.5Al-650 sample and the corresponding carbon concentration and manganese partitioned in blocky austenite and lath-like austenite by EPMA. (a) Micrograph of 1.5Al-650 sample, (b) distribution of carbon and (c) distribution of manganese correspond to the micrograph in figure (a) by EPMA, (d) micrograph of 1.5Al-650 sample, (e) Carbon-concentration and (f) Manganese-concentration correspond to the micrograph in figure (d) by EPMA.

Tables

Table 1. Chemical composition (wt. %) of two experimental steels.

Table 2. Vickers microhardness of constituent phases.

Table 3. Comparisons of other medium Mn TRIP steels and the experimental steels.

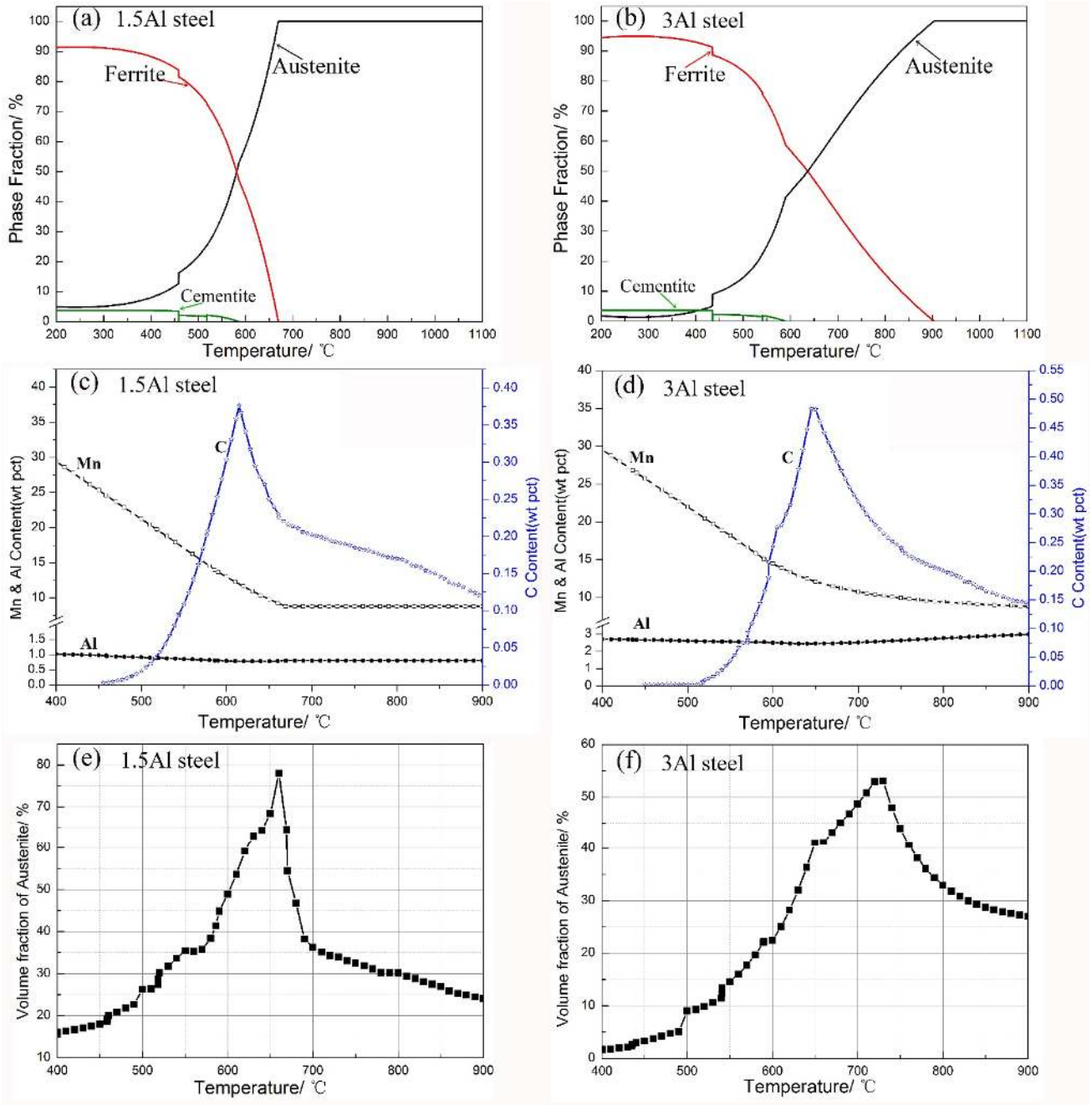

Fig. 1. Schematic illustration of the predictive model development for austenite stabilization as a function of temperature for 1.5Al steel and 3Al steel. (a)-(b) phase fractions, (c)-(d) C, Al and Mn-content in austenite and (e)-(f) calculated retained austenite fractions.

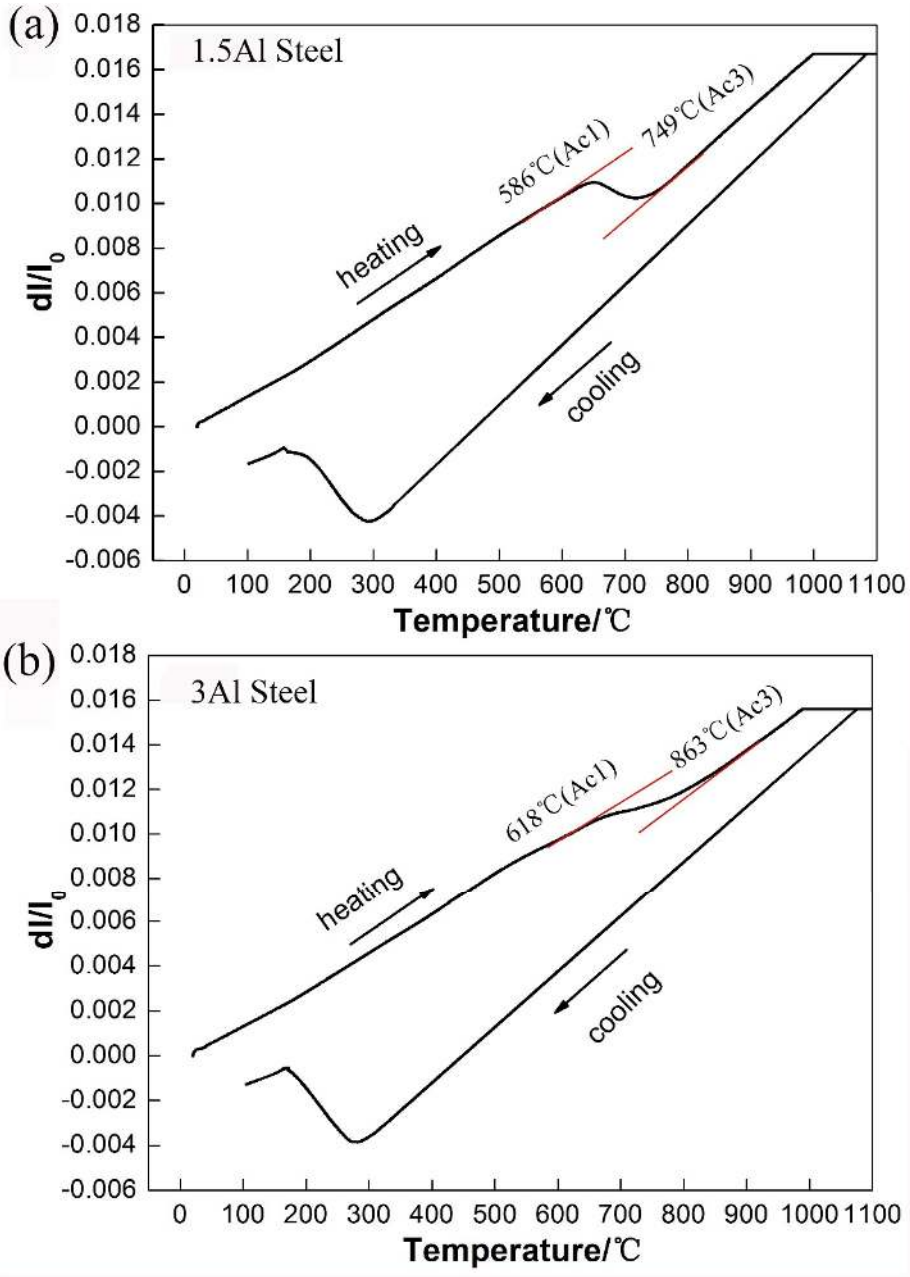

Fig. 2. Dilatometric plots for the experimental steels. (a) 1.5Al steel and (b) 3Al steel.

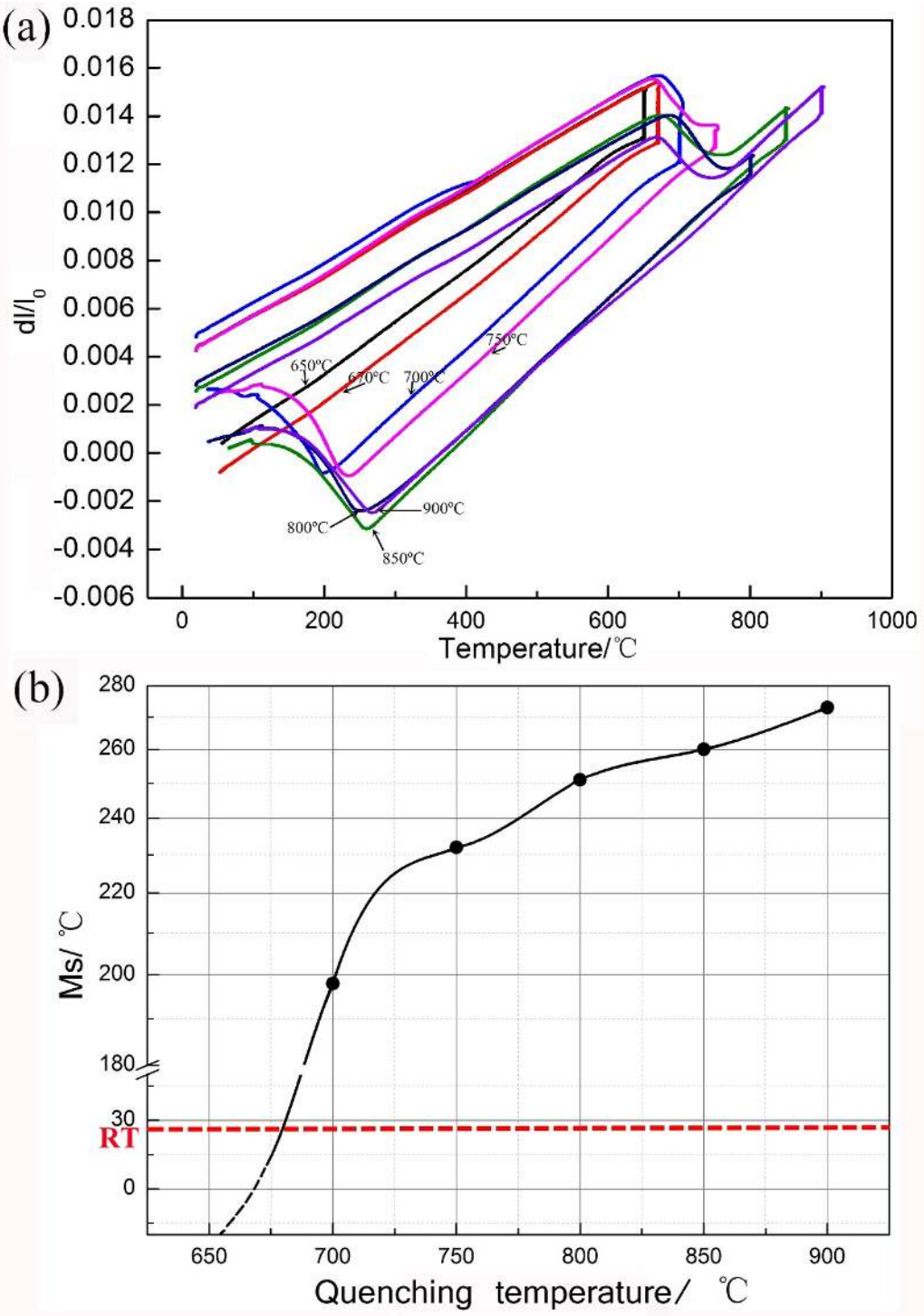

Fig. 3. Dilatometric plots and the evolution of *Ms* for 1.5Al steel on quenching from 650℃, 670℃, 700℃, 750℃, 800℃, 850℃and 900℃. (a) dilatometric plots and (b) evolution of *Ms*.

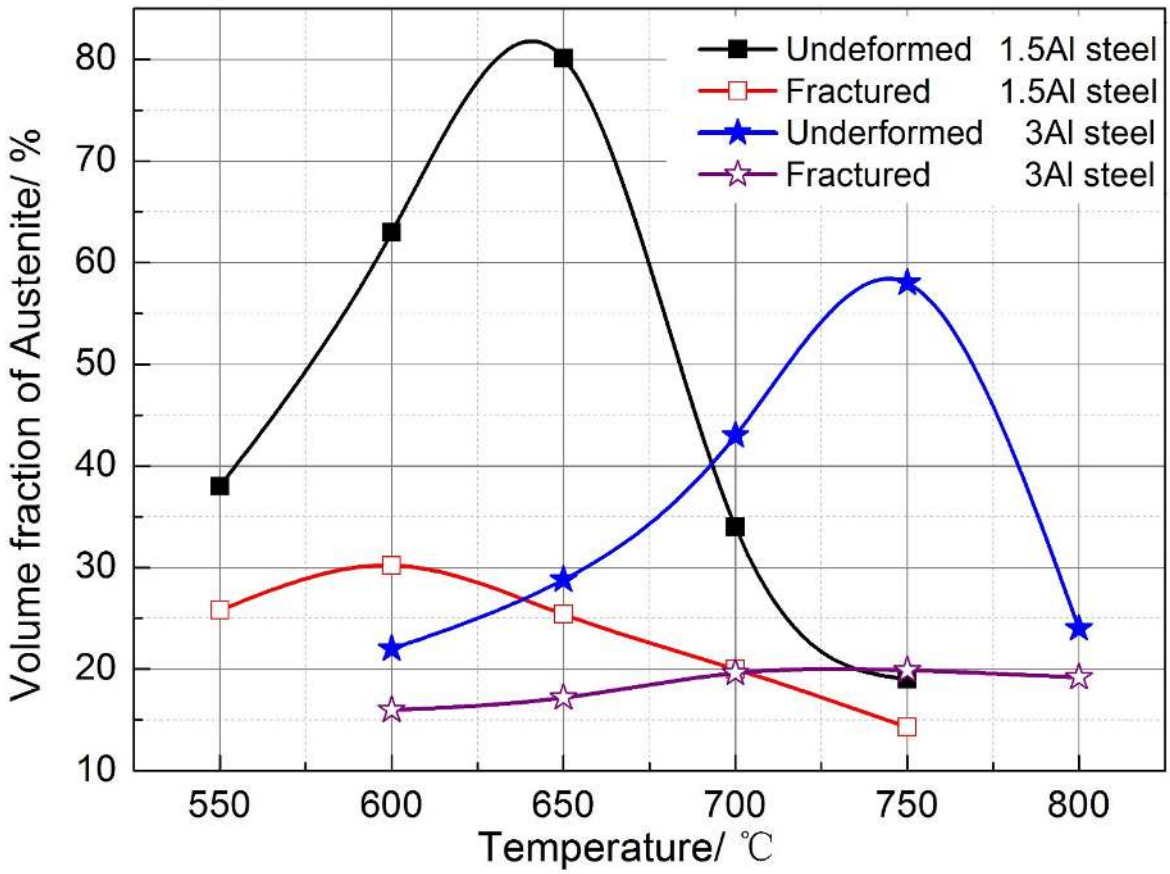

Fig. 4. Austenite fraction in undeformed and fractured samples of 1.5Al steel and 3Al steel heat-treated at different temperatures.

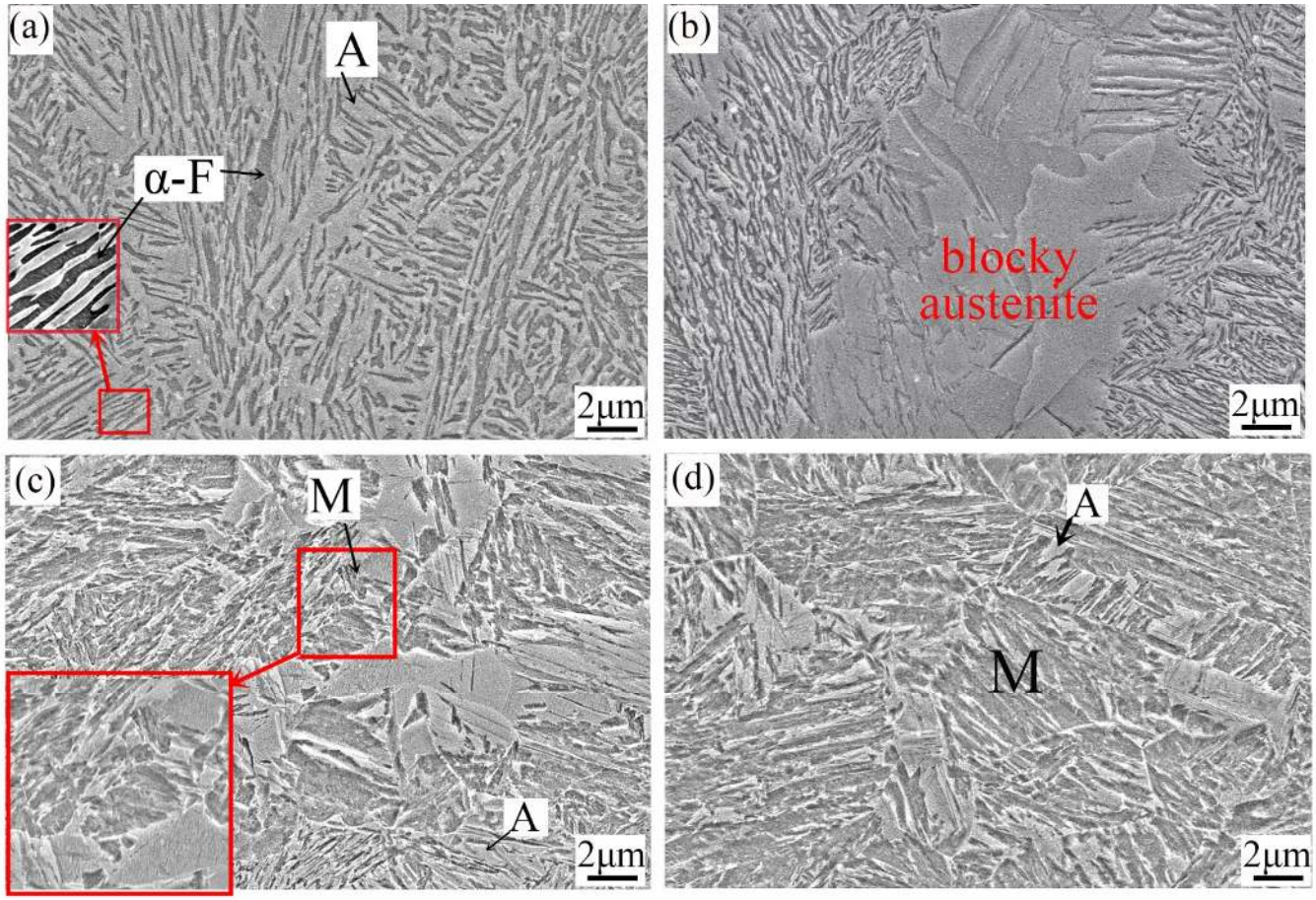

Fig. 5. SEM micrographs of hot-rolled 1.5Al samples after quenching from different temperatures. (a) 600℃, (b) 650℃, (c) 700℃ and (d) 750℃.

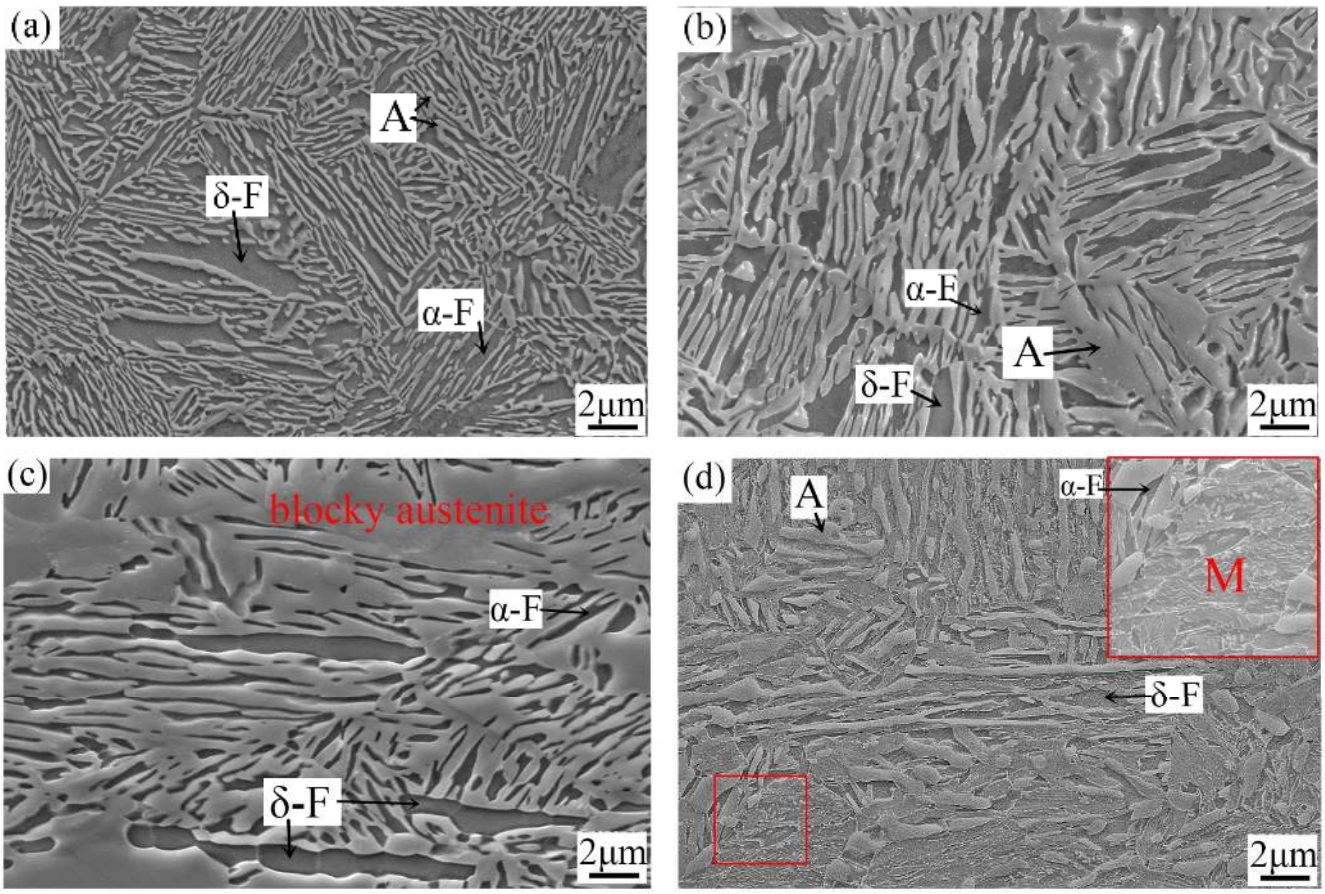

Fig. 6. SEM micrographs of hot-rolled 3Al samples after quenching from different temperatures. (a) 650℃, (b) 700℃, (c) 750℃ and (d) 800℃.

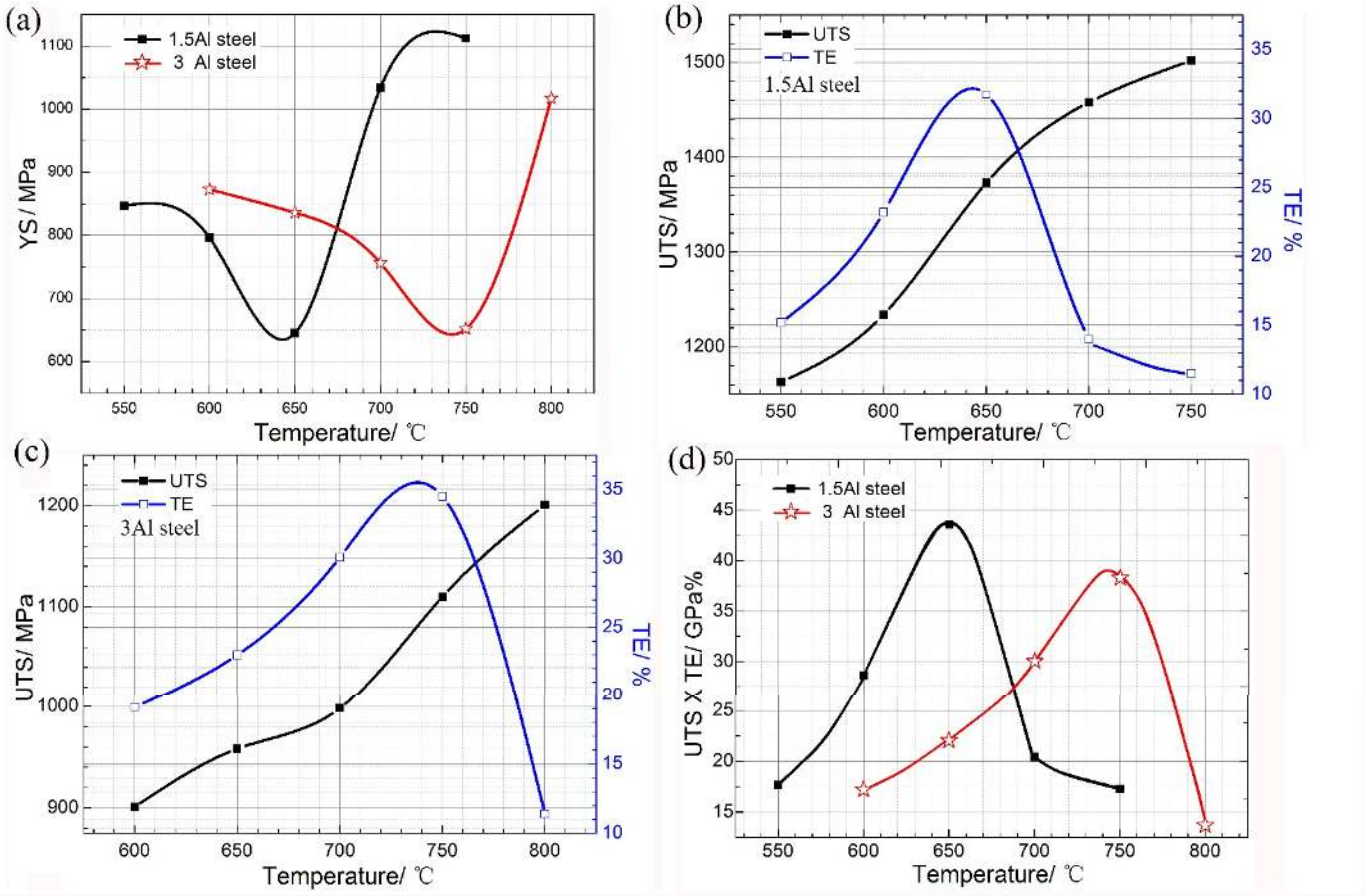

Fig. 7. Comparisons of tensile properties between 1.5Al steel and 3Al steel. (a) YS of the 1.5 Al steel and 3Al steel, (b) UTS and TE of 1.5Al steel, (c) UTS and TE of 3Al steel and (d) UTS × TE comparisons of the 1.5 Al steel and 3Al steel. (YS-yield strength, UTS-ultimate tensile strength, TE-total elongation)

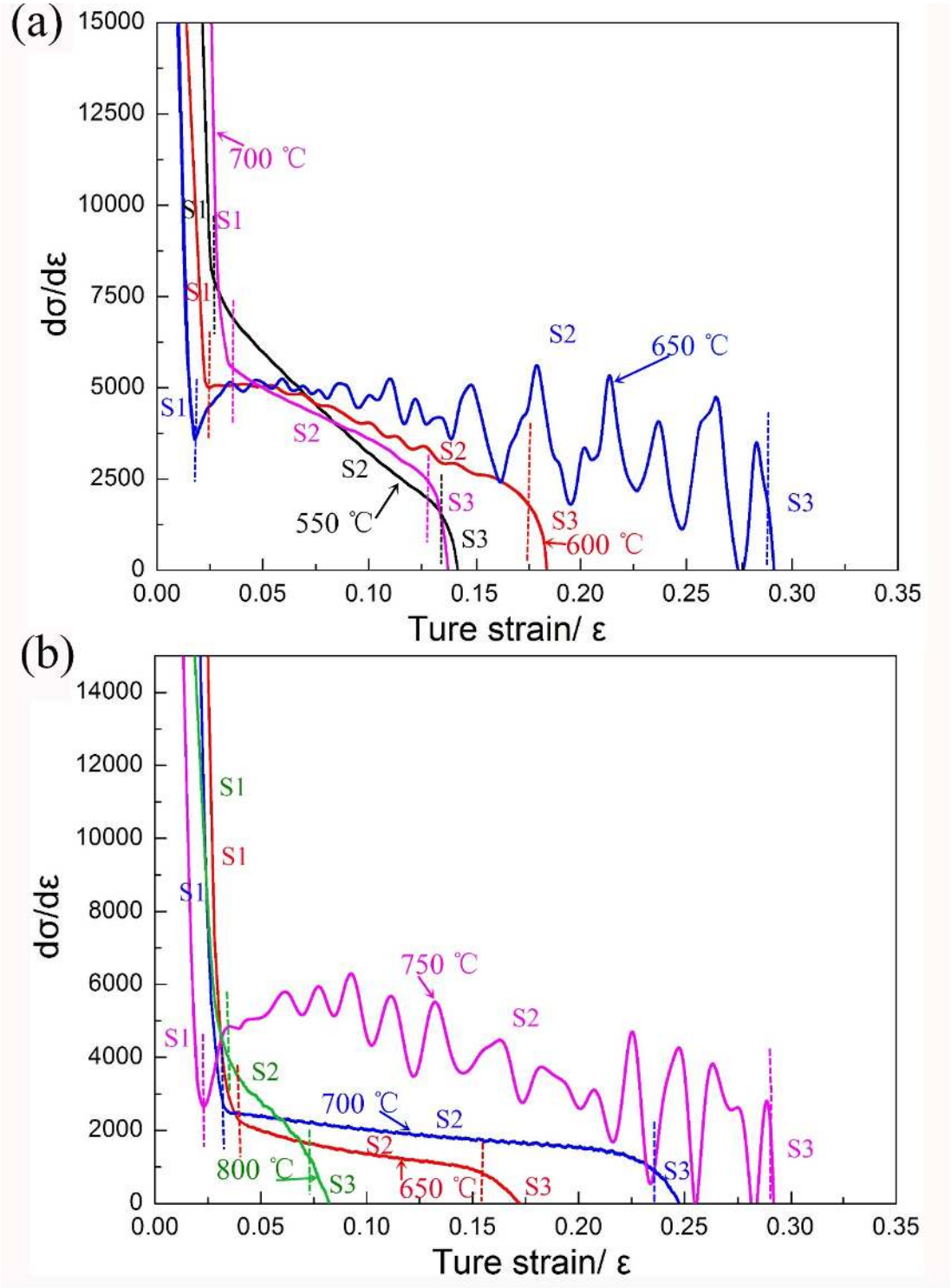

Fig. 8. Work hardening rate of 1.5Al, 3Al steels quenched from different temperatures. (a) 1.5Al steel and (b) 3Al steel.

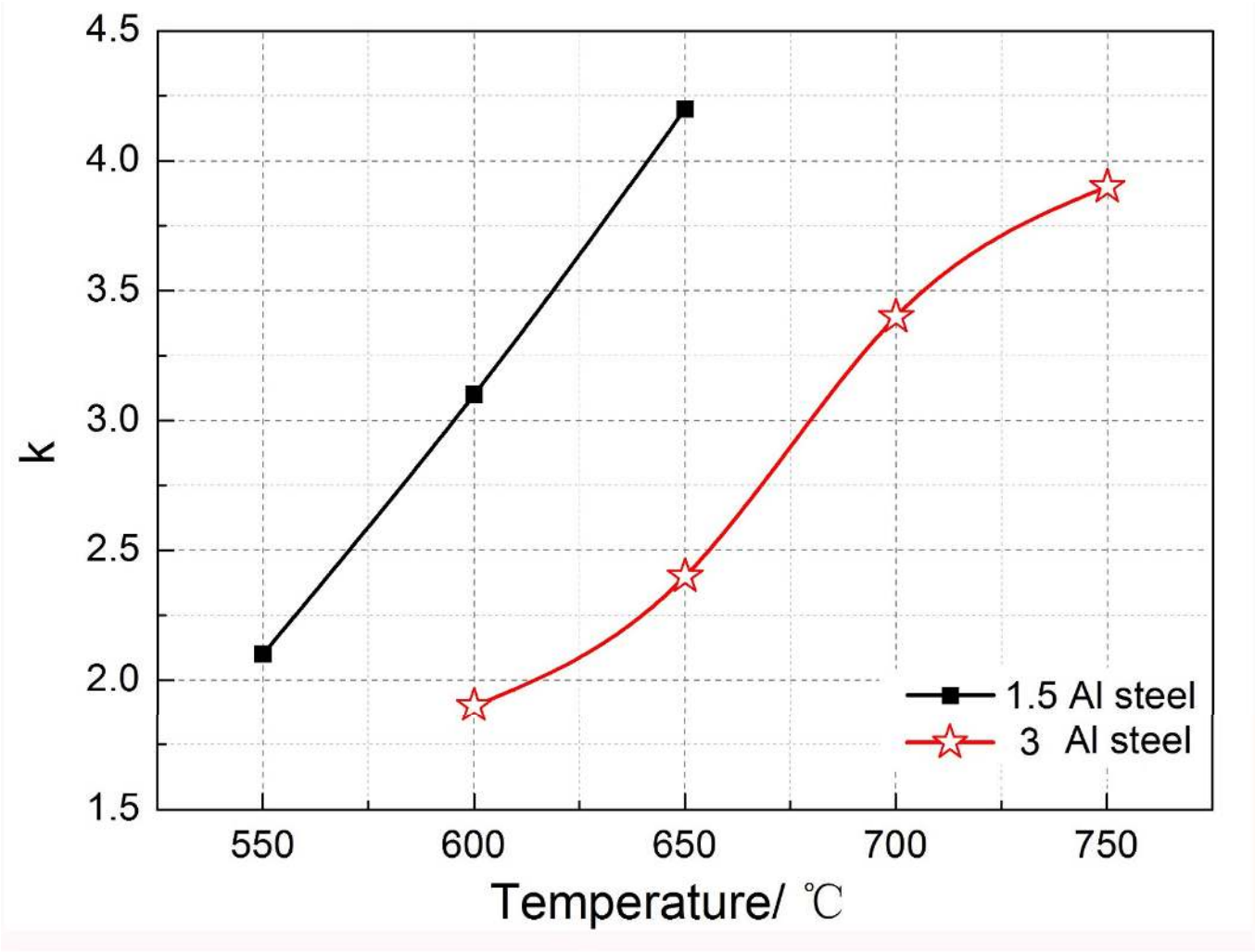

Fig. 9. The plots of parameter *k* for 1.5Al and 3Al steel samples intercritically hardened at different temperatures.

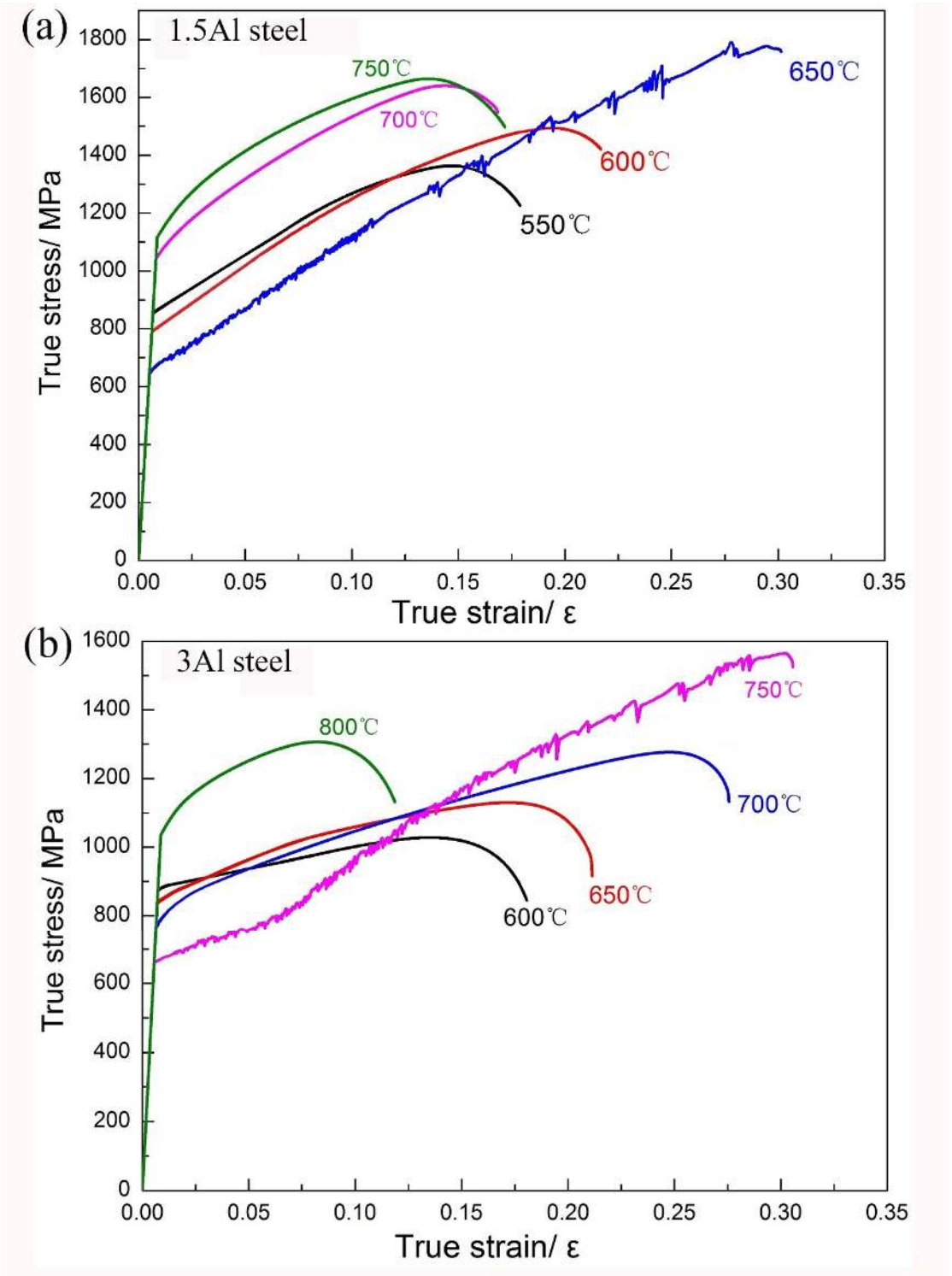

Fig. 10. True strain-stress plots of 1.5Al steel and 3Al steel quenched from different temperatures. (a) 1.5Al steel and (b) 3Al steel.

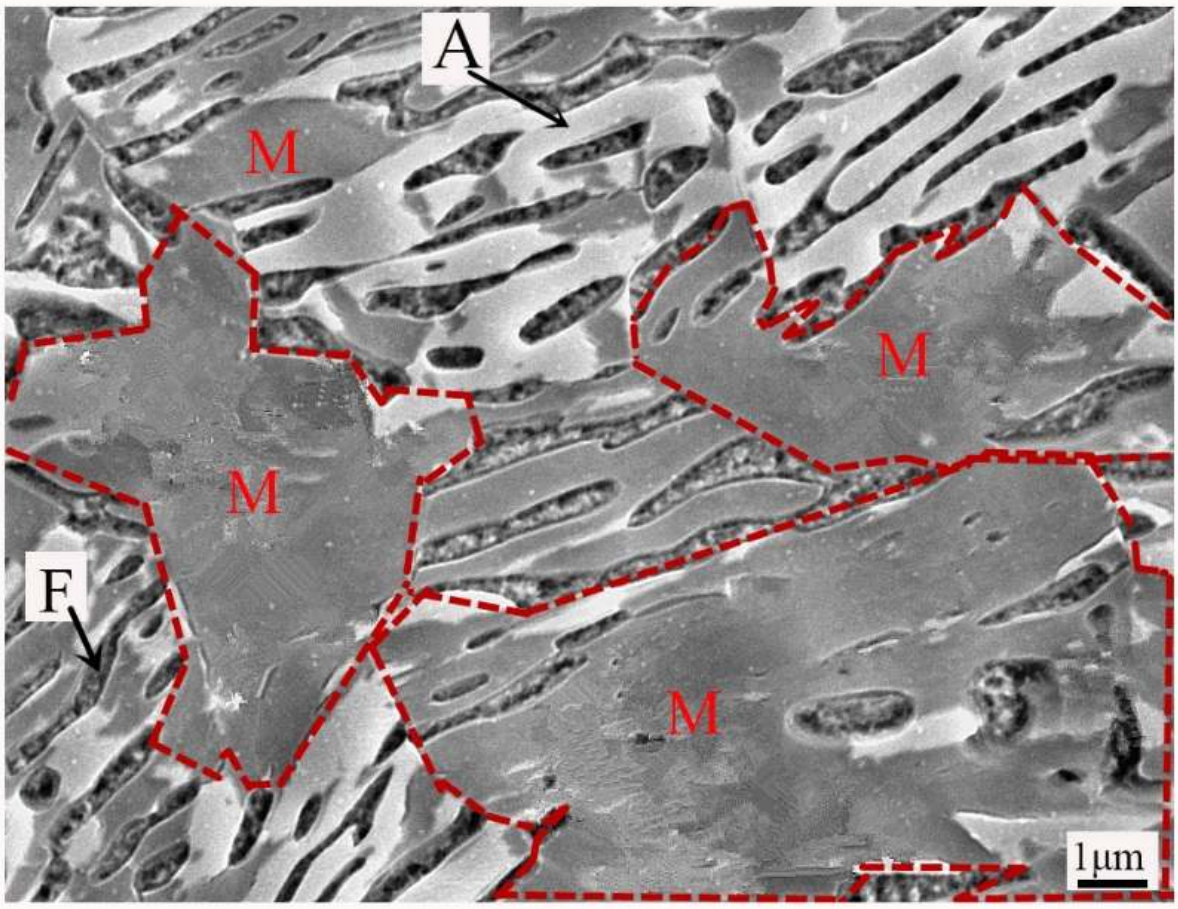

Fig. 11. SEM micrograph of 1.5Al-650 sample after tensile fracture.

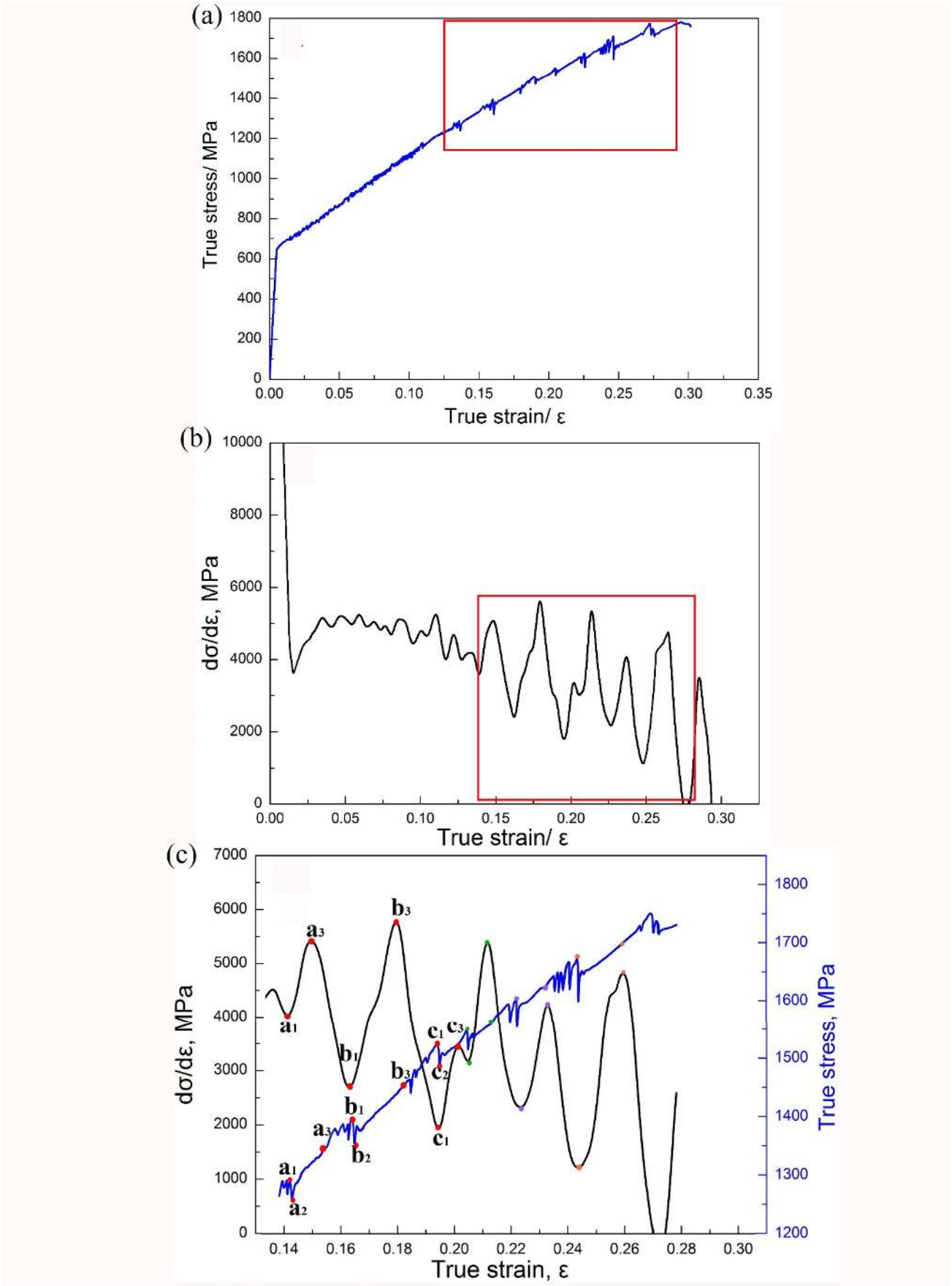

Fig. 12. True stress-strain curve and work-hardening rate plot of 1.5Al-650 sample: (a) true stress-strain curve, (b) work-hardening rate and (c) partial magnification of the true stress-strain and work-hardening rate plots.

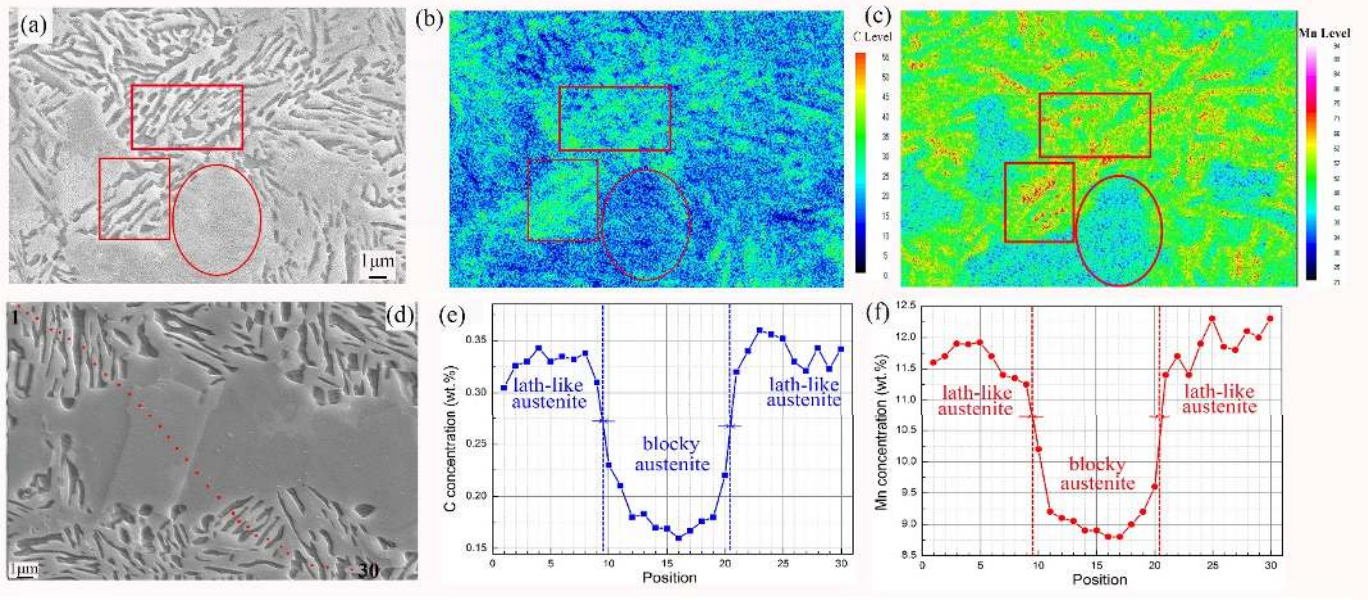

Fig. 13. Micrograph of 1.5Al-650 sample and the corresponding carbon concentration and manganese partitioned in blocky austenite and lath-like austenite by EPMA. (a) Micrograph of 1.5Al-650 sample, (b) distribution of carbon and (c) distribution of manganese correspond to the micrograph in figure (a) by EPMA, (d) micrograph of 1.5Al-650 sample, (e) Carbon-concentration and (f) Manganese-concentration correspond to the micrograph in figure (d) by EPMA.

Table 1. Chemical composition (wt. %) of two experimental steels.

	Al	C	Mn	Fe
1.5Al	1.58	0.22	8.60	Bal
3Al	3.11	0.18	8.34	Bal

Table 2. Vickers microhardness of constituent phases.

Phases	Vickers hardness, HV
α-ferrite	319 ± 15
δ-ferrite	256 ± 8
Austenite	223 ± 10
Martensite (original)	478 ± 10
Martensite (newly generated)	564 ± 15

Table 3. Comparisons of other medium Mn TRIP steels and the experimental steels.

Composition	Initial condition	UTS(MPa)	TE(%)	PSE(GPa%)	Reference
0.13C-6Mn-0.5Si-3.1Al	CR-annealing	854/1161	21.7/12.4	18.5/14.4	15
0.1C-7.1Mn	HR-annealing(80h)	1074	33.6	36.1	12
0.1C-7Mn	CR-annealing	1018	32	32.5	12
0.2C-8Mn-4Al	HR-QT(1h)	980	33	32.3	16
0.2C-11Mn-4Al	HR-QT(1h)	1082/1201	19.8/34.6	23.8/37.5	23
0.2C-8.5Mn-3Al	HR-QT(1h)	1110	34.5	38.3	present work
0.2C-8.5Mn-1.5Al	HR-QT(1h)	1373	31.8	43.6	present work

CR-cold rolled, HR-hot rolled, QT-quenching and tempering, UTS-ultimate tensile strength, TE-total elongation, PSE-product of strength and elongation.